

Scattering-Independent Anomalous Nernst Effect in Ferromagnets

Jürgen Weischenberg,^{1,*} Frank Freimuth,¹ Stefan Blügel,¹ and Yuriy Mokrousov¹

¹*Peter Grünberg Institut and Institute for Advanced Simulation,
Forschungszentrum Jülich and JARA, 52425 Jülich, Germany*

(Dated: November 29, 2021)

Using the full-potential linearized augmented plane-wave method within the density functional theory, we compute all contributions to the scattering independent part of the thermoelectric conductivity tensor $\hat{\alpha}$, namely the intrinsic contribution $\hat{\alpha}^{\text{ic}}$ and the side-jump contribution $\hat{\alpha}^{\text{sj}}$. For the ferromagnetic materials bcc Fe, hcp Co, fcc Ni and $L1_0$ ordered alloys FePd and FePt, our investigations of the energy and temperature dependence of the intrinsic and side-jump contributions show that they are both of equal importance. Overall, our calculations are able to correctly reproduce the order of magnitude and sign of the experimentally measured signal, suggesting that the scattering independent part plays an important role in the anomalous Nernst effect of ferromagnets.

PACS numbers:

When a thermal gradient is applied to a single-domain ferromagnetic material, the anomalous Nernst effect (ANE) shows itself as an electric field \mathbf{E} that emerges in a direction perpendicular to the applied thermal gradient $-\nabla T$ and perpendicular to the sample's magnetization \mathbf{M} .¹ Prominently, the Nernst signal can be used as a probing tool for the vortex phase in type II superconductors^{2,3} and it has been also discussed in spinel ferromagnets⁴ and on a surface of a topological insulator.⁵ However, despite increasing interest in this phenomenon in the past years,⁶ no attempt to predict from first principles the values of the ANE in metallic ferromagnets, such as bcc Fe, has been made so far.

It is convenient to quantify the ANE in terms of the thermoelectric conductivity tensor $\hat{\alpha}$, also called the Peltier or Nernst conductivity tensor. In linear response theory, the expression for the charge current \mathbf{j} in the presence of a weak electric field and a small thermal gradient reads⁷

$$\mathbf{j} = \hat{\sigma} \cdot \mathbf{E} - \hat{\alpha} \cdot \nabla T, \quad (1)$$

where the electric conductivity tensor is denoted by $\hat{\sigma}$. The matrix elements of $\hat{\alpha}$ and $\hat{\sigma}$ are related via the generalized Mott formula⁸⁻¹⁰

$$\hat{\alpha} = -\frac{1}{e} \int d\varepsilon \frac{\partial f}{\partial \mu} \hat{\sigma} \frac{\varepsilon - \mu}{T}, \quad (2)$$

where $e = -|e|$ is the electronic charge, ε the energy and μ the chemical potential of the electrons which appears in the Fermi distribution function $f(\varepsilon, \mu, T)$. In ferromagnetic materials, we can replace the off-diagonal matrix elements of the conductivity tensor with the transverse anomalous Hall conductivity σ^{AHE} ,¹¹ which is usually decomposed into an intrinsic Berry curvature driven contribution σ^{ic} ,¹² and two extrinsic, stemming from disorder, contributions. Of the latter two, the first is the so-called side-jump contribution σ^{sj} , which is caused by the scattering of electrons off impurities but which paradoxically does not depend on their concentration n_i .¹³ The second disorder-driven contribution is the skew-scattering σ^{sk} ,

which is inversely proportional to the impurity concentration, i.e., $\sigma^{\text{sk}} \propto 1/n_i$.^{14,15} The Mott relation, Eq. (2), implies that the thermoelectric conductivity tensor can be decomposed in an analogous way:

$$\hat{\alpha} = \hat{\alpha}^{\text{ic}} + \hat{\alpha}^{\text{sj}} + \hat{\alpha}^{\text{sk}}. \quad (3)$$

The difficulties in understanding the origins of the anomalous Hall effect (AHE) have greatly impeded the progress in the field of the ANE as well. For example, on the side of qualitative theory of solids, we are aware of only a single estimate for the value of $\hat{\alpha}^{\text{ic}}$ in the cuprate $\text{CuCr}_2\text{Se}_{4-x}\text{Br}_x$.¹⁶ However, as we have recently shown, all scattering independent contributions to the AHE, that is, $\hat{\sigma}^{\text{ic}}$ and $\hat{\sigma}^{\text{sj}}$, can be calculated from first principles on an equal footing from the knowledge of the electronic structure of the pristine crystal alone.¹⁷ Since skew scattering is suppressed for metals outside the extremely pure regime,^{18,19} the calculated values for $\hat{\sigma}^{\text{ic}}$ and $\hat{\sigma}^{\text{sj}}$ allow for a quantitative comparison between theory and experiment. In the present work, we extend this methodology to the ANE. We calculate all the scattering-independent contributions to the thermoelectric conductivity tensor, $\hat{\alpha}^{\text{ic}}$ and $\hat{\alpha}^{\text{sj}}$, in bcc Fe, hcp Co, fcc Ni and $L1_0$ ordered alloys FePd and FePt. By comparison to experimental data, we show that $\hat{\alpha}^{\text{ic}}$ and $\hat{\alpha}^{\text{sj}}$ provide the correct order of magnitude and sign of the anomalous Nernst signal in transition-metal ferromagnets. We also make predictions concerning the temperature dependence of the scattering-independent ANE.

Our approach is based on electronic structure calculations performed within the full-potential linearized augmented plane-wave method as implemented in the Jülich density functional theory code FLEUR.²⁰ The matrix elements of the multi-band Bloch Hamiltonian $\hat{H}(\mathbf{k})$ in the basis of maximally-localized Wannier functions^{21,22} have been computed using the Wannier interpolation technique²³ and inserted into the equations for $\hat{\sigma}^{\text{ic}}$ and $\hat{\sigma}^{\text{sj}}$ obtained within the Kubo-Středa formalism,²⁴ assuming short-range disorder in the system.²⁵ The knowledge of any free parameters is not required in this scheme. For the evaluation of the integral in Eq. (2), we adopted an

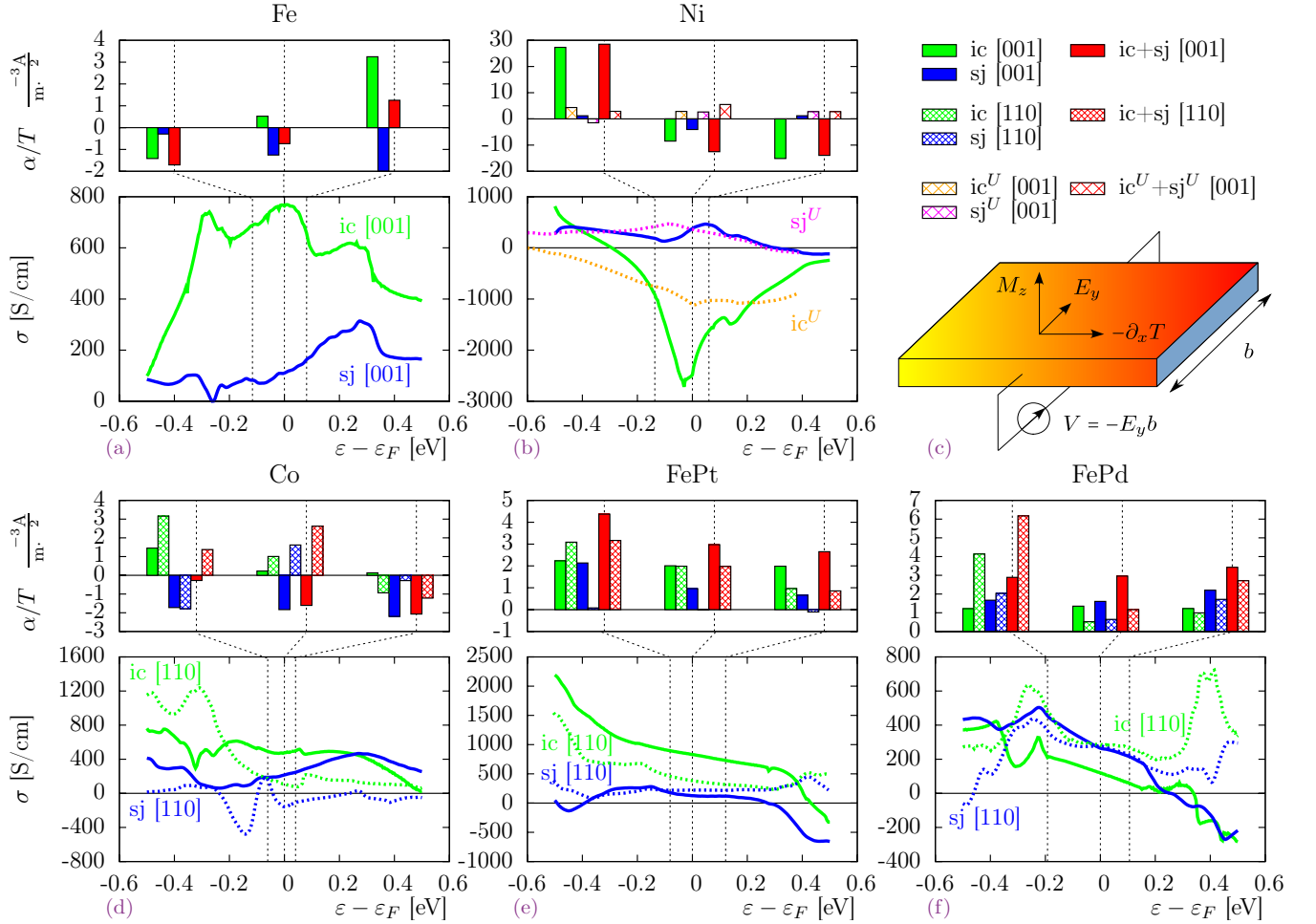


FIG. 1: (Color online) ANE at $T = 300$ K in Fe, Ni, Co, FePt and FePd for different magnetization directions. The bar diagrams in the first row of (a), (b), (d)-(f) show the values of $\alpha = \alpha^{ic} + \alpha^{sj}$ at different energy positions. The true Fermi energy level in each material lies at the position of the middle vertical line. The line diagrams in the lower row of (a), (b), (d)-(f) depict the energy dependence of $\sigma = \sigma^{ic} + \sigma^{sj}$. In (b), hatched bars and dotted lines stand for GGA+ U calculations in Ni with $U = 3.9$ eV and $J = 1.1$ eV. In (d)-(f), hatched bars and dotted lines stand for calculations in Co, FePt and FePd with the magnetization pointing along the [110] direction. A sketch of the experimental setup is shown in (c).

energy grid that was denser at low temperatures, since the energy derivative of the Fermi function becomes a δ -distribution in this limit. Near room temperature, we found that an energy spacing of $\Delta\varepsilon \approx 5$ meV offered the best trade-off between accuracy and computational cost, leading to an error of about 2% for $\hat{\alpha}$.

It follows from an argument by Berger²⁶ that large values for the components of $\hat{\alpha}$ could not arise if electrons of different energies experienced an AHE of the same magnitude and sign, since the transverse velocities of electrons diffusing down the applied temperature gradient would then cancel with those of the less energetic electrons diffusing up the temperature gradient and the net transverse current would be zero. The same can also be deduced from the Mott formula Eq. (2): Since the product $(\partial_\mu f) \cdot (\varepsilon - \mu)$ is an antisymmetric function with respect to the Fermi energy level $\varepsilon_F = \mu$, the ANE would vanish if the AHE conductivity σ^{AHE} was a symmetric

function around ε_F , i.e., if it was equal for a pair of energy values with the same distance to ε_F .

In Fig. 1(a), (b), (d)-(f), the component $\sigma \equiv \boldsymbol{\sigma} \cdot \hat{\mathbf{M}}$ of the anomalous Hall vector $\boldsymbol{\sigma}$ and the component $\alpha \equiv \boldsymbol{\alpha} \cdot \hat{\mathbf{M}}$ of the thermoelectric conductivity vector $\boldsymbol{\alpha}$ parallel to the magnetization direction $\hat{\mathbf{M}} \equiv \mathbf{M}/|\mathbf{M}|$ are shown. They have been computed from Eq. (2) at room temperature as a function of the Fermi energy level in Fe, Ni, Co, FePt and FePd. For the [001] magnetization direction, σ and α correspond to the tensor elements σ_{xy} and α_{xy} , while for the [110] magnetization direction, they correspond to the tensor elements $(\sigma_{yz} + \sigma_{zx})/\sqrt{2}$ and $(\alpha_{yz} + \alpha_{zx})/\sqrt{2}$.²⁷ In bcc Fe, we observe that the intrinsic contribution σ^{ic} is nearly symmetric around the Fermi level ε_F , resulting in a rather small value of α^{ic} . If we shift the Fermi energy artificially by +0.08 eV, the course of σ^{ic} gets more asymmetric with respect to the new Fermi energy and the value of α^{ic} increases signif-

icantly by a factor of 6. As a consequence, the total value $\alpha^{\text{ic}} + \alpha^{\text{sj}}$ changes sign and becomes positive. If the Fermi energy level is lowered by -0.12 eV instead, all contributions become negative. In general, we find that the thermoelectric conductivity in Fe, Co and Ni appears to be highly sensitive to the position of the Fermi level, suggesting that the ANE in ferromagnets can be easily tuned by e.g. suitable doping. On the other hand, for the compounds FePd and FePt the Fermi energy dependence of α is much less pronounced.

By now it is established that the side-jump contribution to the AHE is important in FePd whereas the intrinsic AHE is dominant in FePt.^{28,29} As follows from Fig. 1(e-f), this statement also applies to the ANE in these materials, i.e., $\alpha^{\text{sj}}(\varepsilon_F)$ is as large as $\alpha^{\text{ic}}(\varepsilon_F)$ in FePd, but only half of this value in FePt. This crossover behavior is caused by the different spin-orbit interaction strength of Pd and Pt atoms.^{29,30} In Fe and Co, the magnitude of $\alpha^{\text{sj}}(\varepsilon_F)$ is greater than that of $\alpha^{\text{ic}}(\varepsilon_F)$, albeit $\sigma^{\text{sj}}(\varepsilon_F)$ being smaller than $\sigma^{\text{ic}}(\varepsilon_F)$ in both materials.

In analogy to the AHE,³¹ one might suspect that the ANE is highly anisotropic with respect to the direction of the magnetization in the crystal for hcp Co, and $L1_0$ ordered FePd and FePt alloys, due to their uniaxial crystal structure. Indeed, at the Fermi energy, the side-jump contribution α^{sj} switches its sign in Co and is distinctly reduced in FePd and FePt as the direction of the magnetization is changed from [001] to [110] direction. However, the anisotropy of the intrinsic contribution α^{ic} is not that strong. Such a different dependence of α^{ic} and α^{sj} on the magnetization direction may be attributed to the different distribution of σ^{ic} and σ^{sj} in the Brillouin zone of these materials.¹⁷

The ANE in fcc Ni presents an exceptional case, since the theoretical value of the thermoelectric conductivity in this material is much larger than in other considered compounds, see Fig. 1(b). In Ni, the intrinsic anomalous Hall conductivity is sharply peaked near the Fermi energy, and the respective value for the ANE depends on which side of the peak it is evaluated. There are many indications, however, that the large value of σ^{ic} in Ni is mainly an artifact of the local density approximation (LDA) or the

generalized gradient approximation (GGA), because correlation effects among the $3d$ electrons in this material become of crucial importance for its properties.^{17,32,33} For this reason, we have adopted the same approach as in our previous work and took the correlation effects into account within the GGA+ U scheme.³⁴ For the intra-atomic Coulomb repulsion and exchange parameters U and J , we chose values up to 3.9 eV and 1.1 eV, respectively. This choice of parameters has been found to greatly improve the agreement of the calculated AHE in Ni. Fig. 1(b) reveals that correlations have also a significant effect on the energy dependence of σ^{AHE} and α in Ni. We observe that the peak in the intrinsic contribution to the AHE flattens out, whereas the side-jump contribution remains mostly unaffected upon including the U . This can again be understood from the different behavior of the two effects at the Fermi surface.¹⁷ Upon including U , the intrinsic contribution α^{ic} and the side-jump contribution α^{sj} change their sign and the magnitude of the thermoelectric conductivity is greatly reduced.

For comparison with experiment, we consider the situation in which a temperature gradient in \hat{x} direction, $-\partial_x T$, is applied to an electrically isolated sample perpendicular to the magnetization $\mathbf{M} \parallel \hat{z}$, see Fig. 1(c). As a function of the magnetic field strength $|\mathbf{H}| = H_z$ and magnetization $|\mathbf{M}| = M_z$, the Nernst effect obeys a law of the type $E_y/(-\partial_x T) = H_z Q_0 + 4\pi M_z Q_1$, where Q_0 and Q_1 are the ordinary and anomalous Nernst coefficients, respectively.³⁵ However, in ferromagnetic materials, the ordinary Nernst coefficient is very small,³⁶ $Q_0 \ll Q_1$. The remaining coefficient Q_1 is generally measured in a zero-current configuration, $j_x = j_y = 0$, with the boundary condition $\partial_y T = 0$.³⁷ For a spatially uniform sample in an experimental setup as depicted in Fig. 1(c), it holds that $\sigma_{xx} = \sigma_{yy}$, $\sigma_{xy} = -\sigma_{yx}$ and likewise for the components of $\hat{\alpha}$. In this scenario, we obtain from Eq. (1)

$$\begin{aligned} 4\pi M_z Q_1 &= \rho_{xx}(\alpha_{xy} - S\sigma_{xy}) \\ &= \rho_{xx}(\alpha_{xy}^{\text{ic}} - S\sigma_{xy}^{\text{ic}}) + \rho_{xx}(\alpha_{xy}^{\text{sj}} - S\sigma_{xy}^{\text{sj}}), \end{aligned} \quad (4)$$

where $\rho_{xx} = 1/\sigma_{xx}$ is the resistivity of the sample and the so-called Seebeck-coefficient is defined by $S \equiv E_x/\partial_x T = \alpha_{xx}/\sigma_{xx}$. The last line of Eq. (4) may be interpreted as $4\pi M_z(Q_1^{\text{ic}} + Q_1^{\text{sj}})$, where the intrinsic contribution to the anomalous Nernst coefficient is denoted by Q_1^{ic} and the side-jump contribution is denoted by Q_1^{sj} . While the Seebeck-coefficient S describes the conversion of a thermal current into a longitudinal electrical current, the Nernst-coefficient Q_1 is a measure of the corresponding transverse effect. Even though the value of the temperature gradient $-\partial_x T$ and the strength of the magnetic induction B_z do not appear in Eq. (4), they seem to have a great influence on the ANE experimentally.^{38,39} In particular, B_z influences the magnitude of the magnetization and the corresponding electronic structure. However, values for Q_1 , ρ_{xx} , α_{xy} , S , σ_{xy} and M_z were not measured simultaneously in most experiments. We therefore gathered values for the resistivity ρ_{xx} and Seebeck coefficient S from various sources and computed the

TABLE I: Comparison of $Q_1^{\text{ic+sj}}$ with experimental data for Q_1 in units of $10^{-11} \text{V}/(\text{K}\cdot\text{G})$ near room temperature. For Ni, the values of U and J are in eV.

	Q_1^{ic}	Q_1^{sj}	$Q_1^{\text{ic+sj}}$	Q_1 Expt. ²⁷
Fe	-0.52	-0.39	-0.91	-0.81 to -2.08
Co [001]	1.00	0.07	1.07	2.00 to 2.19
[110]	0.24	0.03	0.27	
Ni $U = 0.0, J = 0.0$	-15.12	-1.09	-16.20	3.04 to 7.31
$U = 1.9, J = 1.1$	-4.40	1.98	-2.42	
$U = 3.9, J = 1.1$	-0.28	1.48	1.20	
$U = 3.9, J = 2.6$	0.74	1.90	2.64	
FePt	4.61	1.27	5.88	5.60

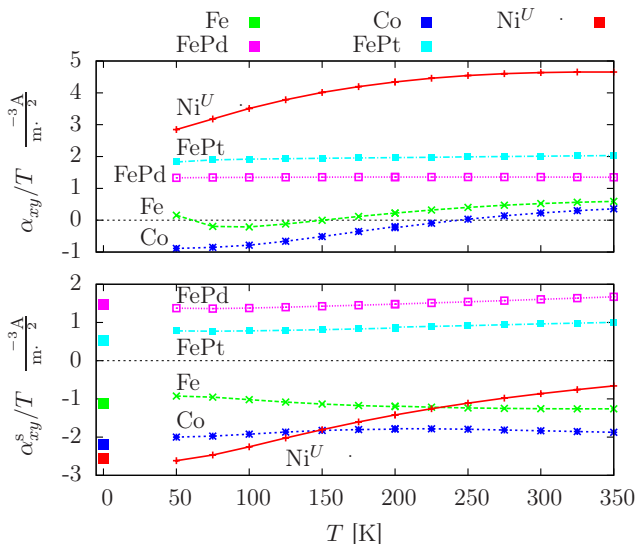


FIG. 2: (Color online) Temperature dependence of the intrinsic- and side-jump contribution to the ANE. The squares at $T = 0$ K stand for the values of α_{xy}^{sj}/T computed from Eq. (5).

scattering-independent contribution $Q_1^{ic+sj} = Q_1^{ic} + Q_1^{sj}$ to the anomalous Nernst coefficient following Eq. (4) (Details of this procedure can be found in the supplement).²⁷

A comparison of our calculated values with experimental data is presented in Tab. (I). The experimental values show a considerable spread, which reflects the fact that the ANE is found to depend sensitively on experimental details and material-specific parameters. Nevertheless, it can clearly be seen that the inclusion of the side-jump contribution is crucial for Fe and FePt and lets theory and experiment match very well: Q_1^{ic+sj} is about 112% of the smaller experimental value in Fe and 105% of the experimental value in FePt. For Co, the side-jump contribution to Q_1^{ic+sj} is relatively small and only around 10% for both magnetization directions, but it still brings the theoretical value for the anomalous Nernst coefficient closer to experiment. The lack of better agreement may be due to the fact that for the Seebeck coefficient in Co solely experimental data for polycrystalline samples has been available, but the corresponding value for monocrystalline samples should be inserted into Eq. (4) instead. Remarkably, when the magnetization is changed from [001] into [110] direction, the sign change of α^{sj} in Co at the Fermi energy level is compensated by the sign change of σ^{sj} , and the net contribution Q_1^{sj} stays roughly the same. For Ni, the value calculated in bare GGA differs drastically from experiment, and even has the wrong sign. However, when the value of U is increased within GGA+ U , the calculated value approaches the experimental result in magnitude and sign. This suggests that the main reason for the discrepancy between experiment and theory in Ni originates from an inadequate description of the electronic structure in the vicinity of the Fermi energy level within GGA.⁴⁰

Overall, the values in Tab. (I) demonstrate that the

intrinsic- and side-jump contribution play an important role in the ANE of ferromagnets. This finding is consistent with earlier studies in this field, which examined the behavior of the anomalous Nernst coefficient Q_1 as a function of the resistivity ρ_{xx} . As far as the scattering-independent contributions are concerned, one would expect a linear dependence of the form $Q_1/T \propto \rho_{xx}$,²⁶ which is also observed in experiment.^{41–45} Our work substantiates these observations with quantitative analysis.

The calculated temperature dependence of the thermoelectric conductivity tensor for [001] magnetization direction is depicted in Fig. (2). α_{xy}^{ic} is positive at 300 K, but changes its sign in Fe and Co as the temperature is decreased. Below 50 K, it becomes positive again in Fe. The importance of the side-jump contribution to the ANE is stressed by the fact that for considered materials α_{xy}^{sj} is of the same order of magnitude or even larger than α_{xy}^{ic} . In contrast to the intrinsic contribution, α_{xy}^{sj} does not change its sign. While the temperature dependence of α_{xy}^{sj}/T is almost absent in FePd and FePt, it ranges from $-2.6 \cdot 10^{-3} \text{ A}/(\text{m}\cdot\text{K}^2)$ at $T = 50$ K to $-0.7 \cdot 10^{-3} \text{ A}/(\text{m}\cdot\text{K}^2)$ at $T = 350$ K in Ni.

In the zero temperature limit, one can apply the Sommerfeld expansion to the integral in Eq. (2) to obtain the standard Mott formula which relates the ANE to the energy derivative of the AHE:⁴⁶

$$\frac{\alpha_{xy}}{T} = -\frac{\pi^2 k_B^2}{3e} \left[\frac{d\sigma_{xy}}{d\varepsilon} \right]_{\varepsilon=\varepsilon_F}. \quad (5)$$

For the intrinsic Nernst effect, it is known that the above formula may be violated as $T \rightarrow 0$ K.⁶ Indeed, we find that the energy derivative of the intrinsic contribution converges only very slowly with respect to the number of \mathbf{k} -points in the Brillouin zone that are used for the evaluation of σ^{ic} . The slow convergence is due to the sensitivity of the Berry curvature to the position of the Fermi energy, especially when the latter approaches avoided band crossings or points of band degeneracy.⁴⁷ However, for the side-jump contribution, Mott's formula Eq. (5) holds, as can be seen by interpolating the curves in Fig. (2) to $T = 0$ K. Apart from Ni, it yields a rather good estimate for the value of α_{xy}^{sj}/T at room temperature as well.

In summary, we presented the *ab initio* calculations of the scattering independent contributions to the ANE in several ferromagnets. The theoretical values for the thermoelectric conductivity tensor and the comparison of the calculated anomalous Nernst coefficient with experiment suggests that the ANE in elementary Fe, Co, Ni, in the ferromagnetic alloy FePt and presumably also in FePd is largely caused by the intrinsic and side-jump mechanisms. Discrepancies between theory and experiment in Ni are likely due to the imprecise description of correlation effects within bare GGA, which can be remedied by GGA+ U calculations.

We thank J. Sinova for fruitful discussions and gratefully acknowledge Jülich Supercomputing Centre for computing time as well as funding by the HGF-YIG pro-

gramme VH-NG-513. J. W. was supported under grant SPP 1538 SpinCaT by the German Science Foundation.

- * Corresp. author: j.weischenberg@fz-juelich.de
- ¹ W. Nernst, *Ann. Physik* **267**, 760 (1887).
 - ² Z. A. Xu, N. P. Ong, Y. Wang, T. Kakeshita, and S. Uchida, *Nature* **406**, 486 (2000).
 - ³ Y. Wang, Z. A. Xu, T. Kakeshita, S. Uchida, S. Ono, Y. Ando, and N. P. Ong, *Phys. Rev. B* **64**, 224519 (2001).
 - ⁴ W.-L. Lee, S. Watauchi, V. L. Miller, R. J. Cava, and N. P. Ong, *Phys. Rev. Lett.* **93**, 226601 (2004).
 - ⁵ T. Yokoyama and S. Murakami, *Phys. Rev. B* **83**, 161407 (2011).
 - ⁶ D. L. Bergman and V. Oganesyan, *Phys. Rev. Lett.* **104**, 066601 (2010).
 - ⁷ J. M. Luttinger, *Phys. Rev.* **135**, A1505 (1964).
 - ⁸ L. Smrčka and P. Středa, *J. Phys. C: Solid State Phys.* **10**, 2153 (1977).
 - ⁹ M. Jonson and G. D. Mahan, *Phys. Rev. B* **21**, 4223 (1980).
 - ¹⁰ M. J. Kearney and P. N. Butcher, *J. Phys. C: Solid State Phys.* **21**, L265 (1988).
 - ¹¹ E. M. Pugh, *Phys. Rev.* **36**, 1503 (1930).
 - ¹² R. Karplus and J. M. Luttinger, *Phys. Rev.* **95**, 1154 (1954).
 - ¹³ L. Berger, *Phys. Rev. B* **2**, 4559 (1970).
 - ¹⁴ J. Smit, *Physica* **21**, 877 (1955).
 - ¹⁵ J. Smit, *Physica* **24**, 39 (1958).
 - ¹⁶ D. Xiao, Y. Yao, Z. Fang, and Q. Niu, *Phys. Rev. Lett.* **97**, 026603 (2006).
 - ¹⁷ J. Weischenberg, F. Freimuth, J. Sinova, S. Blügel, and Y. Mokrousov, *Phys. Rev. Lett.* **107**, 106601 (2011).
 - ¹⁸ T. Miyasato, N. Abe, T. Fujii, A. Asamitsu, S. Onoda, Y. Onose, N. Nagaosa, and Y. Tokura, *Phys. Rev. Lett.* **99**, 086602 (2007).
 - ¹⁹ N. Nagaosa, J. Sinova, S. Onoda, A. H. MacDonald, and N. P. Ong, *Rev. Mod. Phys.* **82**, 1539 (2010).
 - ²⁰ FLEUR web page, description see <http://www.flapw.de>.
 - ²¹ F. Freimuth, Y. Mokrousov, D. Wortmann, S. Heinze, and S. Blügel, *Phys. Rev. B* **78**, 035120 (2008).
 - ²² A. A. Mostofi, J. R. Yates, Y.-S. Lee, I. Souza, D. Vanderbilt, and N. Marzari, *Comput. Phys. Comm.* **178**, 685 (2008).
 - ²³ J. R. Yates, X. Wang, D. Vanderbilt, and I. Souza, *Phys. Rev. B* **75**, 195121 (2007).
 - ²⁴ P. Středa and L. Smrčka, *phys. stat. sol. (b)* **70**, 537 (1975).
 - ²⁵ A. A. Kovalev, J. Sinova, and Y. Tserkovnyak, *Phys. Rev. Lett.* **105**, 036601 (2010).
 - ²⁶ L. Berger, *Phys. Rev. B* **5**, 1862 (1972).
 - ²⁷ See supplementary material at [URL will be inserted here] for further information.
 - ²⁸ P. He, L. Ma, Z. Shi, G. Y. Guo, J.-G. Zheng, Y. Xin, and S. M. Zhou, *Phys. Rev. Lett.* **109**, 066402 (2012).
 - ²⁹ K. M. Seemann, Y. Mokrousov, A. Aziz, J. Miguel, F. Kronast, W. Kuch, M. G. Blamire, A. T. Hindmarch, B. J. Hickey, I. Souza, and C. H. Marrows, *Phys. Rev. Lett.* **104**, 076402 (2010).
 - ³⁰ H. Zhang, F. Freimuth, S. Blügel, Y. Mokrousov, and I. Souza, *Phys. Rev. Lett.* **106**, 117202 (2011).
 - ³¹ H. Zhang, S. Blügel, and Y. Mokrousov, *Phys. Rev. B* **84**, 024401 (2011).
 - ³² I. Yang, S. Y. Savrasov, and G. Kotliar, *Phys. Rev. Lett.* **87**, 216405 (2001).
 - ³³ H.-R. Fuh and G.-Y. Guo, *Phys. Rev. B* **84**, 144427 (2011).
 - ³⁴ A. B. Shick, A. I. Liechtenstein, and W. E. Pickett, *Phys. Rev. B* **60**, 10763 (1999).
 - ³⁵ J.-P. Jan, in *Solid State Physics*, Vol. 5, edited by F. Seitz and D. Turnbull (Academic Press, 1957) pp. 1 – 96.
 - ³⁶ G. S. Nielsen, *Philos. Mag. Series 7* **18**, 575 (1934).
 - ³⁷ E. H. Butler and E. M. Pugh, *Phys. Rev.* **57**, 916 (1940).
 - ³⁸ L. L. Campbell, *Phys. Rev. (Series I)* **26**, 416 (1908).
 - ³⁹ L. L. Campbell, *Galvanomagnetic and thermomagnetic effects* (Longmans, Green and co., 1923).
 - ⁴⁰ Further reasons for the discrepancy might be the temperature dependence of the electronic structure or details of dynamical Coulomb screening of *d*-electrons in Ni, etc.
 - ⁴¹ I. Campbell, *J. Magn. Magn. Mater.* **12**, 31 (1979).
 - ⁴² T. Luciński and J. Baszyński, *J. Magn. Magn. Mater.* **127**, 57 (1993).
 - ⁴³ E. I. Kondorskii and R. P. Vasileva, *Soviet Phys. JETP* **18**, 277 (1964).
 - ⁴⁴ A. Cheremushkina and R. P. Vasileva, *Sov. Phys. Solid State* **8**, 659 (1966).
 - ⁴⁵ R. P. Vasil'eva and B. Akmuradov, *Russ. Phys. J.* **15**, 814 (1972).
 - ⁴⁶ N. W. Ashcroft and D. N. Mermin, *Solid State Physics* (Saunders College Publishing, 1988).
 - ⁴⁷ Y. Yao, L. Kleinman, A. H. MacDonald, J. Sinova, T. Jungwirth, D.-s. Wang, E. Wang, and Q. Niu, *Phys. Rev. Lett.* **92**, 037204 (2004).

Supplement

Jürgen Weischenberg,^{1,*} Frank Freimuth,¹ Stefan Blügel,¹ and Yuriy Mokrousov¹

¹*Peter Grünberg Institut & Institute for Advanced Simulation,
Forschungszentrum Jülich and JARA, 52425 Jülich, Germany*

(Dated: November 29, 2021)

We compare the theoretical value of the anomalous Nernst coefficient Q_1 with experimental data. For this purpose, we need the values of the resistivity $\hat{\rho}$, the thermoelectric conductivity tensor $\hat{\alpha}$, the Seebeck coefficient S , the conductivity $\hat{\sigma}$ and the magnetization \mathbf{M} . In linear transport theory, the temperature dependent transport coefficients $\sigma_{ij} = e\mathcal{L}_{ij}^{(0)}$ and $\alpha_{ij} = \mathcal{L}_{ij}^{(1)}/T$ can be computed from the formula

$$\mathcal{L}_{ij}^{(n)}(T) = -\frac{1}{e} \int d\varepsilon \frac{\partial f(\varepsilon, \mu, T)}{\partial \mu} \cdot \sigma_{ij}^{T=0}(\varepsilon) \cdot (\varepsilon - \mu)^n, \quad (1)$$

where the expression for the Fermi distribution function is given by $f(\varepsilon, \mu, T) = 1/[\exp((\varepsilon - \mu)/k_B T) + 1]$. Since the derivate $\partial f/\partial \mu$ decays exponentially, the integrand in Eq. (1) needs only be evaluated in an interval of about ± 0.5 eV around the Fermi energy level. For $\sigma_{xy}^{T=0}$ we insert the anomalous Hall conductivity $\sigma^{\text{AHE}} = \sigma^{\text{ic}} + \sigma^{\text{sj}}$, which can be computed from the electronic structure of the pristine crystal alone with the same method as developed in Ref. (1). In our electronic structure calculations we have chosen a plane-wave cutoff K_{max} of 3.8 bohr^{-1} and constructed a set of 18 maximally localised Wannier functions per atom on a uniform $8 \times 8 \times 8$ grid of *ab initio* \mathbf{k} -points using the WANNIER90 code and our interface between FLEUR and WANNIER90.^{2,3} The actual calculation of σ^{AHE} has then been performed on a very dense grid of up to $800 \times 800 \times 800$ \mathbf{k} -points using the Wannier interpolation scheme.⁴

For $|\mathbf{M}|$ we take the saturation magnetization at room temperature. Since the Curie temperature T_C for Fe, Co and Ni is quite large, $T_C \gg 300$ K, we suppose that the temperature dependence of $|\mathbf{M}|$ has no significant effect on the calculated values for $Q_1^{\text{ic+sj}}$. For a general magnetization along $\hat{\mathbf{M}} \equiv \mathbf{M}/|\mathbf{M}|$, we introduce the anomalous Hall vector $\boldsymbol{\sigma}$ and the thermoelectric conductivity vector $\boldsymbol{\alpha}$,

$$[\boldsymbol{\sigma}]_i \equiv \frac{1}{2} \epsilon_{ijk} \sigma_{jk}, \quad \boldsymbol{\sigma} = \begin{pmatrix} \sigma_{yz} \\ \sigma_{zx} \\ \sigma_{xy} \end{pmatrix}, \quad [\boldsymbol{\alpha}]_i \equiv \frac{1}{2} \epsilon_{ijk} \alpha_{jk}, \quad \boldsymbol{\alpha} = \begin{pmatrix} \alpha_{yz} \\ \alpha_{zx} \\ \alpha_{xy} \end{pmatrix}, \quad (2)$$

where ϵ_{ijk} are the components of the Levi-Civita tensor. These vectors can be decomposed into a part which is parallel and into a part which is perpendicular to $\hat{\mathbf{M}}$,

$$\boldsymbol{\sigma} = \sigma_{\parallel} \hat{\mathbf{M}} + \boldsymbol{\sigma}_{\perp}, \quad \boldsymbol{\alpha} = \alpha_{\parallel} \hat{\mathbf{M}} + \boldsymbol{\alpha}_{\perp}. \quad (3)$$

In the above equation, $\hat{\mathbf{n}}$ denotes the unit vector perpendicular to $\hat{\mathbf{M}}$. In single crystals, $\boldsymbol{\sigma}$, $\boldsymbol{\alpha}$ and \mathbf{M} are perfectly colinear only when \mathbf{M} points into special high-symmetry directions. For the [001] magnetization direction, it has been shown in the main text that the anomalous Nernst coefficient can be computed via the equation

$$Q_1 = \rho_{xx}(\alpha_{xy} - S\sigma_{xy})/4\pi M_z. \quad (4)$$

For other magnetization directions, we replace $\hat{\sigma}_{xy}$ with the parallel component $\sigma = \boldsymbol{\sigma} \cdot \hat{\mathbf{M}}$ and $\hat{\alpha}_{xy}$ with the parallel component $\alpha = \boldsymbol{\alpha} \cdot \hat{\mathbf{M}}$. For example, if the magnetization points into [110] direction, these correspond to the tensor elements $\sigma = (\sigma_{yz} + \sigma_{zx})/\sqrt{2}$ and $\alpha = (\alpha_{yz} + \alpha_{zx})/\sqrt{2}$, respectively. The anisotropy of $\hat{\rho}$ and S needs also be considered. In hcp Co, in the presence of a magnetic field, the resistivity in the direction of the *c*-axis is about $10.32 \mu\Omega\text{-cm}$, but drops to $5.55 \mu\Omega\text{-cm}$ in the direction perpendicular to this axis.⁵ For the anisotropy of the Seebeck coefficient in hcp Co, no suitable experimental values have been found. We have therefore resorted to data for polycrystalline samples. Presumably, the anisotropy of S in hcp Co is relatively small.⁶

In most experiments, the values of Q_1 , $\hat{\rho}$, S and \mathbf{M} are not measured simultaneously. As illustrated in Fig. (1), we therefore estimate ρ_{xx} and S from linear interpolation whenever their values are not available:

$$\rho_{xx} = a_1 \cdot T + b_1, \quad S = a_2 \cdot T + b_2. \quad (5)$$

The uncertainties in $\hat{\rho}$ and S also affect our prediction of the theoretical values for $Q_1^{\text{ic+sj}}$. However, the spread of the experimental values for Q_1 appears to be much more significant. A comparison of theoretical with experimental data can be found in Tab. (I) and Tab. (II).

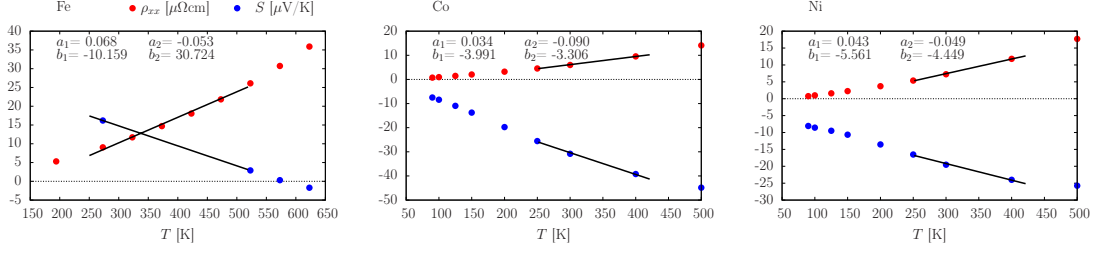


FIG. 1: Interpolation of ρ_{xx} and S for Fe, Co and Ni based on data from Ref. (7–9) for polycrystalline samples.

TABLE I: Comparison with experimental data. Temperature T in K; magnetic field B in G; longitudinal resistivity ρ in $\mu\Omega\cdot\text{cm}$; Seebeck coefficient S in $\mu\text{V}/\text{K}$; transverse anomalous Hall conductivity σ in $1/(\Omega\cdot\text{cm})$; transverse anomalous thermoelectric conductivity α in $10^{-3}\text{A}/(\text{m}\cdot\text{K})$; anomalous Nernst coefficient Q_1 in $10^{-11}\text{V}/(\text{K}\cdot\text{G})$. Values that are labeled by an asterisk are taken from interpolation of data from Ref. (5,7–9). The sign of the values from Ref. (10) has been adjusted to be in accordance with the sign convention of Campbell.¹¹

	T	B	ρ	S	σ^{ic}	α^{ic}/T	σ^{sj}	α^{sj}/T	Q_1^{ic}	Q_1^{sj}	$Q_1^{\text{ic+sj}}$	Q_1 Expt.
Fe	291	6290	9.63*	15.24*	744	0.505	115	-1.254	-0.43	-0.24	-0.67	-1.05 ¹⁰
	293	—	12.55	14.29	744	0.509	115	-1.254	-0.52	-0.30	-0.82	-0.82 ¹²
	313	23000	11.65	14.07*	741	0.544	115	-1.258	-0.46	-0.29	-0.75	-2.04 ¹³
	313	—	13.73	13.70	741	0.544	115	-1.258	-0.52	-0.34	-0.87	-0.90 ¹²
	323	23000	12.21	13.54*	739	0.559	116	-1.260	-0.45	-0.31	-0.76	-2.06 ¹³
	333	18000	12.49*	13.01*	738	0.572	116	-1.260	-0.43	-0.32	-0.76	-0.81 ¹⁴
	333	23000	12.77	13.01*	738	0.572	116	-1.260	-0.44	-0.33	-0.77	-2.08 ¹³
	333	—	14.91	13.07	738	0.572	116	-1.260	-0.52	-0.39	-0.91	-0.98 ¹²
	343	23000	13.33	12.48*	737	0.583	116	-1.261	-0.43	-0.35	-0.78	-2.10 ¹³
Co [001]	297	6290	10.32*	-30.09*	484	0.216	222	-1.831	0.88	0.07	0.95	2.00 ¹⁰
	297	10570	10.32*	-30.09*	484	0.216	222	-1.831	0.88	0.07	0.95	1.80 ¹⁰
	298	9000	10.32*	-30.18*	484	0.220	222	-1.832	0.88	0.07	0.95	1.90 ¹⁵
	300	—	10.32*	-30.36*	484	0.226	222	-1.833	0.89	0.07	0.96	1.80 ¹⁶
	320	9000	10.32*	-32.16*	485	0.286	223	-1.850	0.95	0.07	1.03	2.19 ¹⁵
	333	18000	10.32*	-33.33*	486	0.320	223	-1.861	1.00	0.07	1.07	2.00 ¹⁴
	350	—	10.32*	-34.87*	486	0.359	223	-1.874	1.05	0.07	1.12	2.15 ¹⁶
Co [110]	297	6290	5.55*	-30.09*	125	1.010	-91	1.657	0.21	0.07	0.28	2.00 ¹⁰
	297	10570	5.55*	-30.09*	125	1.010	-91	1.657	0.21	0.07	0.28	1.80 ¹⁰
	298	9000	5.55*	-30.18*	125	1.009	-91	1.644	0.21	0.07	0.28	1.90 ¹⁵
	300	—	5.55*	-30.36*	126	1.007	-90	1.618	0.21	0.07	0.28	1.80 ¹⁶
	320	9000	5.55*	-32.16*	128	0.994	-88	1.359	0.23	0.05	0.27	2.19 ¹⁵
	333	18000	5.55*	-33.33*	130	0.995	-87	1.197	0.24	0.03	0.27	2.00 ¹⁴
	350	—	5.55*	-34.87*	133	1.006	-85	0.994	0.25	0.02	0.27	2.15 ¹⁶
FePt	293	52566	35.90	-12.40	828	2.007	132	0.957	4.61	1.27	5.88	5.60 ¹⁷
Fe	$4\pi M_z = 22100 \text{ G}^{13}$											
Co	$4\pi M_z = 17857 \text{ G}^{18}$											
FePt	$4\pi M_z = 12566 \text{ G}^{17}$											

TABLE II: The same as in Tab. (I) for Ni calculated within the GGA+ U approach. The values of the parameters U and J are given in eV.

	T	B	ρ	S	σ^{ic}	α^{ic}/T	σ^{sj}	α^{sj}/T	Q_1^{ic}	Q_1^{sj}	$Q_1^{\text{ic+sj}}$	Q_1 Expt.
$\text{Ni}_{J=0.0}^{U=0.0}$	291	6290	7.03*	-18.75*	-2150	-9.057	350	-4.169	-8.27	-0.69	-8.96	3.55 ¹⁰
	291	10620	7.03*	-18.75*	-2150	-9.057	350	-4.169	-8.27	-0.69	-8.96	1.30 ¹⁰
	300	—	7.42*	-19.19*	-2140	-8.482	349	-4.034	-8.71	-0.71	-9.42	5.25 ¹⁶
	311	9000	7.90*	-19.73*	-2128	-7.814	347	-3.873	-9.23	-0.72	-9.96	2.59 ¹⁵
	313	6670	12.15	-19.83*	-2126	-7.697	347	-3.844	-14.19	-1.10	-15.30	5.93 ¹³
	323	6670	12.63	-20.32*	-2115	-7.129	345	-3.702	-14.70	-1.10	-15.80	6.62 ¹³
	330	9000	8.72*	-20.66*	-2107	-6.750	344	-3.604	-10.12	-0.74	-10.86	3.04 ¹⁵
	333	6670	13.04	-20.81*	-2104	-6.591	343	-3.563	-15.12	-1.09	-16.20	7.31 ¹³
	343	6670	13.46	-21.30*	-2092	-6.081	342	-3.428	-15.53	-1.06	-16.59	8.00 ¹³
	350	9000	9.59*	-21.64*	-2085	-5.740	340	-3.336	-11.03	-0.73	-11.76	3.66 ¹⁵
350	—	9.59*	-21.64*	-2085	-5.740	340	-3.336	-11.03	-0.73	-11.76	7.25 ¹⁶	
$\text{Ni}_{J=1.1}^{U=1.9}$	291	6290	7.03*	-18.75*	-1112	0.999	409	-0.111	-2.23	0.91	-1.31	3.55 ¹⁰
	291	10620	7.03*	-18.75*	-1112	0.999	409	-0.111	-2.23	0.91	-1.31	1.30 ¹⁰
	300	—	7.42*	-19.19*	-1112	1.047	409	-0.078	-2.38	1.00	-1.39	5.25 ¹⁶
	311	9000	7.90*	-19.73*	-1113	1.105	408	-0.039	-2.58	1.10	-1.48	2.59 ¹⁵
	313	6670	12.15	-19.83*	-1113	1.115	408	-0.032	-3.98	1.71	-2.27	5.93 ¹³
	323	6670	12.63	-20.32*	-1114	1.166	408	0.003	-4.20	1.85	-2.35	6.62 ¹³
	330	9000	8.72*	-20.66*	-1114	1.200	408	0.027	-2.93	1.31	-1.62	3.04 ¹⁵
	333	6670	13.04	-20.81*	-1114	1.215	408	0.037	-4.40	1.98	-2.42	7.31 ¹³
	343	6670	13.46	-21.30*	-1115	1.262	408	0.070	-4.61	2.12	-2.49	8.00 ¹³
	350	9000	9.59*	-21.64*	-1115	1.294	408	0.092	-3.32	1.55	-1.77	3.66 ¹⁵
350	—	9.59*	-21.64*	-1115	1.294	408	0.092	-3.32	1.55	-1.77	7.25 ¹⁶	
$\text{Ni}_{J=1.1}^{U=3.9}$	291	6290	7.03*	-18.75*	-801	4.627	430	-0.904	-0.19	0.67	0.48	3.55 ¹⁰
	291	10620	7.03*	-18.75*	-801	4.627	430	-0.904	-0.19	0.67	0.48	1.30 ¹⁰
	300	—	7.42*	-19.19*	-802	4.637	429	-0.863	-0.19	0.74	0.55	5.25 ¹⁶
	311	9000	7.90*	-19.73*	-802	4.647	428	-0.815	-0.19	0.82	0.63	2.59 ¹⁵
	313	6670	12.15	-19.83*	-802	4.648	427	-0.806	-0.29	1.27	0.98	5.93 ¹³
	323	6670	12.63	-20.32*	-803	4.653	426	-0.765	-0.29	1.38	1.09	6.62 ¹³
	330	9000	8.72*	-20.66*	-803	4.656	426	-0.737	-0.19	0.98	0.79	3.04 ¹⁵
	333	6670	13.04	-20.81*	-803	4.656	425	-0.725	-0.28	1.48	1.20	7.31 ¹³
	343	6670	13.46	-21.30*	-804	4.656	424	-0.687	-0.27	1.58	1.31	8.00 ¹³
	350	9000	9.59*	-21.64*	-804	4.655	424	-0.661	-0.19	1.16	0.97	3.66 ¹⁵
350	—	9.59*	-21.64*	-804	4.655	424	-0.661	-0.19	1.16	0.97	7.25 ¹⁶	
$\text{Ni}_{J=2.6}^{U=3.9}$	291	6290	7.03*	-18.75*	-842	6.347	444	-0.379	0.33	0.90	1.23	3.55 ¹⁰
	291	10620	7.03*	-18.75*	-842	6.347	444	-0.379	0.33	0.90	1.23	1.30 ¹⁰
	300	—	7.42*	-19.19*	-843	6.330	443	-0.355	0.37	0.97	1.34	5.25 ¹⁶
	311	9000	7.90*	-19.73*	-844	6.307	443	-0.327	0.41	1.08	1.49	2.59 ¹⁵
	313	6670	12.15	-19.83*	-844	6.302	442	-0.322	0.64	1.66	2.30	5.93 ¹³
	323	6670	12.63	-20.32*	-845	6.276	442	-0.298	0.69	1.79	2.48	6.62 ¹³
	330	9000	8.72*	-20.66*	-846	6.257	441	-0.282	0.49	1.26	1.75	3.04 ¹⁵
	333	6670	13.04	-20.81*	-846	6.248	441	-0.275	0.74	1.90	2.64	7.31 ¹³
	343	6670	13.46	-21.30*	-847	6.218	440	-0.253	0.78	2.02	2.80	8.00 ¹³
	350	9000	9.59*	-21.64*	-847	6.195	439	-0.237	0.57	1.47	2.03	3.66 ¹⁵
350	—	9.59*	-21.64*	-847	6.195	439	-0.237	0.57	1.47	2.03	7.25 ¹⁶	

$$4\pi M_z = 5670 \text{ G}^{13}$$

* corresp. author: j.weischenberg@fz-juelich.de

- ¹ J. Weischenberg, F. Freimuth, J. Sinova, S. Blügel, and Y. Mokrousov, *Phys. Rev. Lett.* **107**, 106601 (2011).
- ² A. A. Mostofi, J. R. Yates, Y.-S. Lee, I. Souza, D. Vanderbilt, and N. Marzari, *Comput. Phys. Comm.* **178**, 685 (2008).
- ³ F. Freimuth, Y. Mokrousov, D. Wortmann, S. Heinze, and S. Blügel, *Phys. Rev. B* **78**, 035120 (2008).
- ⁴ J. R. Yates, X. Wang, D. Vanderbilt, and I. Souza, *Phys. Rev. B* **75**, 195121 (2007).
- ⁵ H. Masumoto, H. Saito, and M. Kikuchi, *Sci. Rep. Res. Inst. Tohoku Univ. Phys. Chem. Metall.* **18**, 84 (1966).
- ⁶ B. Sinha and A. N. Nigam, *Pramana J. Phys.* **36**, 221 (1991).
- ⁷ W. Fulkerson, J. P. Moore, and D. L. McElroy, *J. Appl. Phys.* **37**, 2639 (1966).
- ⁸ M. J. Laubitz and T. Matsumura, *Can. J. Phys.* **51**, 1247 (1973).
- ⁹ M. J. Laubitz, T. Matsumura, and P. J. Kelly, *Can. J. Phys.* **54**, 92 (1976).
- ¹⁰ H. Zahn, *Ann. Physik* **319**, 886 (1904).
- ¹¹ L. L. Campbell, *Galvanomagnetic and thermomagnetic effects* (Longmans, Green and co., 1923).
- ¹² E. Hall and L. L. Campbell, *Proc. Am. Acad.* **46**, 625 (1911).
- ¹³ E. H. Butler and E. M. Pugh, *Phys. Rev.* **57**, 916 (1940).
- ¹⁴ A. W. Smith, *Philos. Mag. Series 6* **31**, 367 (1916).
- ¹⁵ E. H. Hall, *Phys. Rev.* **26**, 820 (1925).
- ¹⁶ A. W. Smith, *Phys. Rev. (Series I)* **33**, 295 (1911).
- ¹⁷ M. Mizuguchi, S. Ohata, K. Uchida, E. Saitoh, and K. Takanashi, *Appl. Phys. Express* **5**, 093002 (2012).
- ¹⁸ W. W. Stifler, *Phys. Rev. (Series I)* **33**, 268 (1911).